ACS APPLIED MATERIALS & INTERFACES

Research Article

www.acsami.org

Surface Modification of Multipass Caliber-Rolled Ti Alloy with Dexamethasone-Loaded Graphene for Dental Applications

Ho Sang Jung,[†,§] Taekyung Lee,[‡,§] Il Keun Kwon,[⊥] Hyoung Seop Kim,[†] Sei Kwang Hahn,*[,†] and Chong Soo Lee*[,†,#]

[†]Department of Materials Science and Engineering, Pohang University of Science and Technology (POSTECH), 77 Cheongam-ro, Nam-gu, Pohang, Kyungbuk, 790-784, Korea

[‡]Department of Mechanical Engineering, Northwestern University, 2145 Sheridan Road, Evanston, Illinois 60208-3111, United States

[#]Graduate Institute of Ferrous Technology (GIFT), Pohang University of Science and Technology (POSTECH), 77 Cheongam-ro, Nam-gu, Pohang, Kyungbuk 790-784, Korea

[⊥]Department of Maxillofacial Biomedical Engineering and Institute of Oral Biology, School of Dentistry, Kyung Hee University, Seoul 130-701, Korea

Supporting Information

ABSTRACT: Titanium (Ti) and its alloys with a high mechanical strength and a small diameter can be effectively exploited for minimally invasive dental implantation. Here, we report a multipass caliber-rolled Ti alloy of Ti13Nb13Zr (MPCR-TNZ) with a high mechanical strength and strong fatigue characteristics. For further dental applications, MPCR-TNZ was surface-modified with reduced graphene oxide (RGO) and loaded with osteogenic dexamethasone (Dex) via $\pi-\pi$ stacking on the graphitic domain of RGO. The Dex-loaded RGO-MPCR-TNZ (Dex/RGO-MPCR-TNZ) resulted in significantly enhanced growth and differentiation of MC3T3-E1 cells into osteoblasts, which was confirmed by Alizarin red staining, alkaline phosphatase activity test, immunocytochemistry, and real-time PCR. Moreover, we could confirm the feasibility of Dex/RGO-MPCR-TNZ from the implantation test of a prototype of a dental implant to an artificial bone block for clinical dental applications.

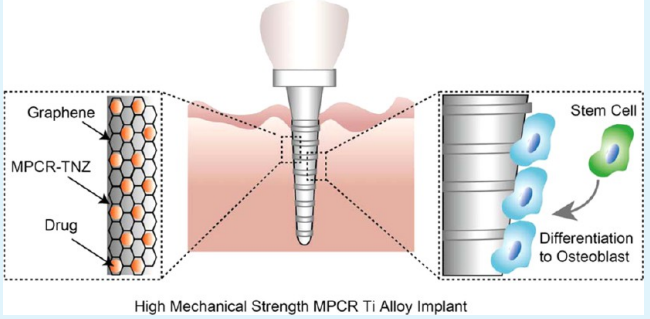

KEYWORDS: *graphene, titanium alloy, $\pi-\pi$ stacking, dental implant, osseointegration*

1. INTRODUCTION

Titanium (Ti) and its alloys have been widely used in the field of implant materials due to its corrosion resistance and excellent biocompatibility.[1] Especially, Ti alloys with a high mechanical strength and a small diameter can be effectively exploited for minimally invasive dental implantation. Fatigue resistance is another indispensable characteristic for the long-term and repetitive loading to the materials after dental implantation. The multipass caliber-rolling (MPCR) is a plastic deformation process to induce an ultrafine-grained (UFG) structure with an average grain size less than 1 μm. This process has proved its effectiveness in the field of structural materials such as steels.[2−6] For the first time, we reported the application of the MPCR process to Ti alloys for biomedical applications.[7] We paid particular attention to Ti13Nb13Zr (TNZ) alloy registered in the ASTM F1713-08 standard for surgical implants. The solution-treated (ST), and solution-treated and aged (STA) TNZ alloys showed better biomechanical properties than current implant materials of commercially pure titanium (CP-Ti). The MPCR process could enhance these properties of Ti alloys even more.[7]

Graphene is a sp2-bonded two-dimensional carbon material which has unique mechanical, optical, and electrical properties.[8,9] Graphene has recently attracted a great deal of attention for biomedical applications such as drug delivery,[10] biosensing,[11] and tissue engineering.[12] For drug delivery, it was reported that a high amount of drugs containing π-electrons or hydrophobic drugs could be effectively loaded on the graphene surface.[13] In particular, the differentiation of mesenchymal stem cells (MSCs) into osteoblasts was greatly enhanced on the graphene substrate synthesized by chemical vapor deposition (CVD).[14] It was also reported that the adsorbed drugs on graphene could facilitate the osteogenic differentiation of MSCs due to the increased local concentration.[13] However, it is hard to transfer graphene synthesized by CVD on complicated 3D structures, especially screw shaped dental implants. For biomedical applications of graphene as a biologically active surface in the body, graphene needs to be easily coated on the

Received: February 5, 2015
Accepted: April 24, 2015
Published: April 24, 2015

DOI: 10.1021/acsami.5b03431
ACS Appl. Mater. Interfaces 2015, 7, 9598−9607

surface of 3D structures with reasonable durability and stability after implantation.

In this work, a multipass caliber-rolled Ti alloy of Ti13Nb13Zr (MPCR-TNZ) was prepared with a high mechanical strength and strong fatigue characteristics for dental implant applications. After that, reduced graphene oxide (RGO) was coated on the disc-shaped MPCR-TNZ (RGO-MPCR-TNZ), which was loaded with an osteogenic drug of dexamethasone (Dex)[15] for facilitated osseointegration. After characterization by atomic force microscopy (AFM), X-ray photoelectron spectroscopy (XPS), and Raman spectroscopy, the effect of Dex/RGO-MPCR-TNZ was assessed on the differentiation of MC3T3-E1 preosteoblasts into osteoblasts. For further applications, a prototype dental implant of Dex/RGO-MPCR-TNZ was fabricated and implanted to an artificial bone block for the assessment of the graphene surface stability by Raman spectroscopy and scanning electron microscopy (SEM) with the analysis of dynamic fatigue property.

2. EXPERIMENTAL SECTION

Preparation of MPCR-TNZ. TNZ rods were prepared with a diameter of 28 mm. The β-transus temperature of this alloy (T_β) is known to be 742 °C.[16] The rods were solution-treated (ST) at 800 °C for 1 h and then water-quenched to prepare ST-TNZ. Sections of ST-TNZ were subsequently heated at 500 °C for 6 h according to the ASTM F1713−08 standard to prepare STA-TNZ. Other sections were heated in a furnace at 650 °C for 1 h and then deformed via MPCR process with an area reduction of ca. 90% to fabricate MPCR-TNZ.

Microstructural analysis of MPCR-TNZ. The microstructure of MPCR-TNZ was analyzed using disc samples with a diameter of 8 mm and a thickness of 1 mm. The bare materials were wet-abraded using SiC papers with a grit size up to #2400, mirror-polished using a clean cloth with 1-μm alumina powder, and cleaned with acetone in an ultrasonic bath. These samples were electro-polished at 22 V in a solution of 2-butoxyethanol (245 mL), 60% $HClO_4$ (40 mL), and methanol (410 mL) to investigate phase and grain structures by electron backscatter diffraction (EBSD). Then, the discs were mirror-polished again and used to measure the contact angle.

Evaluation of mechanical properties of bare materials. Tensile specimens were machined using ST-TNZ, STA-TNZ, and MPCR-TNZ with a gauge diameter of 5 mm and a gauge length of 10 mm. Tensile tests were performed at a strain rate of 5×10^{-3} s^{-1} in ambient atmosphere. The tests were repeated three times with an extensometer to obtain reliable mechanical data. Young's modulus was measured by the free resonance method using the disc samples described above. Fatigue tests were performed using specimens with a gauge diameter of 3 mm and a gauge length of 6 mm. Vickers hardness tests were carried out with a load of 2 kg_f for 10 s. The test was repeated 15 times for each sample to obtain statistically meaningful data.

RGO coating on MPCR-TNZ. Mirror-polished and piranha-treated MPCR-TNZ was immersed in 3% solution of (3-aminopropyl)-triethoxysilane (APTES) in ethanol for 1 h to introduce positive amine groups on the material surface. After washing with ethanol and distilled water thrice, 4 mg/mL of graphene oxide (GO) solution with a size of 0.3−2 μm was spin-coated on the MPCR-TNZ surface at 100 rpm for 5 s following 2,000 rpm for 30 s to obtain GO-coated MPCR-TNZ with a uniform thickness. RGO-MPCR-TNZ was obtained by reducing in hydrazine vapor for 24 h. This material was washed with enough fresh distilled water to remove the remaining hydrazine.

Characterization of RGO-MPCR-TNZ. The morphology of MPCR-TNZ and RGO-MPCR-TNZ was characterized by tapping-mode atomic force microscope (AFM, Veeco Multimode Scanning Probe Microscope with the NanoScope IV Controller, Santa Barbara, CA). Raman spectroscopy of MPCR-TNZ and RGO-MPCR-TNZ was compared at D band (1350 cm^{-1}) and G band (1580 cm^{-1}) with a confocal Raman Spectroscope Alpha 300R (Witec, Ulm, Germany). Carbon-peak analysis for various oxidized carbon states was performed by X-ray photoelectron spectroscopy (XPS) (ESCALAB 250, Thermo VG Scientific, West Sussex, UK). Contact angles of ST-TNZ, STA-TNZ, MPCR-TNZ, RGO-MPCR-TNZ, and bovine serum-incubated RGO-MPCR-TNZ were measured thrice using a contact angle analyzer (SmartDrop, Femtofab, Korea).

***In vitro* drug release test.** Drug was loaded on RGO-MPCR-TNZ in the dark for 24 h using 1 mg/mL of DEX dissolved in DMSO and diluted in PBS (1:10). All the supernatant was collected and the loading content was calculated using the Dex standard curve obtained at 260 nm by UV−vis spectroscopy (Eppendorf Biospectrophotometer, Eppendorf AG, Hamburg, Germany). Unabsorbed Dex was removed by washing with PBS thrice. *In vitro* drug release test was conducted using Dex/RGO-MPCR-TNZ immersed in 1 mL of PBS at 37 °C in a shaking incubator for 7 days. After incubation for 1, 2, 4, 48, 72, 96, 120, and 168 h, 10 μL of PBS was collected and replaced with 10 μL of fresh PBS. The released amount of Dex was determined by the Dex standard curve at 260 nm considering the replaced PBS volume.

Cytotoxicity assessment and cell growth monitoring. Before cell culture, all the samples were sterilized by immersing in 70% ethanol for 10 min. After drying under UV lamp in the clean bench for more than 4 h, the cytocompatibility of ST-TNZ, STA-TNZ, MPCR-TNZ, and RGO-MPCR-TNZ was assessed by MTT assay. MC3T3-E1 cells at a density of 2×10^4 were cultured on each sample for 72 h. After that, media was exchanged with serum-free media and 2 mg/mL of MTT solution was added in each well. The media was replaced with DMSO after 2 h and the absorbance was measured at 520 nm with a microplate reader (EMax microplate reader, Bucher Biotec AG, Basel, Switzerland). The growth of undifferentiated MC3T3-E1 cells was monitored by MTT assay on MPCR-TNZ and RGO-MPCR-TNZ after culture for 1 day, 3 days, and 7 days. In addition, the morphology of MC3T3-E1 cells cultured on MPCR-TNZ, RGO-MPCR-TNZ, and Dex/RGO-MPCR-TNZ for 7 days was analyzed with a HR FE-SEM (JEOL JSM-7401F, JEOL, Tokyo, Japan).

MC3T3-E1 cell differentiation. To study osteogenic differentiation, preosteoblast of MC3T3-E1 cells at passage #5 (subclone 4) was cultured at a density of 2×10^4 in a 24-well cell culture flask containing MPCR-TNZ, RGO-MPCR-TNZ, and Dex/RGO-MPCR-TNZ. Osteogenic media of α-MEM containing 10 mM of glycerol 2-phosphate and 0.2 mM of ascorbic acid (without Dex) was replaced every day for a week. Nonosteogenic media was replaced for nondifferentiation groups.

Characterization of MC3T3-E1 cell differentiation. The calcium deposition of MC3T3-E1 cells cultured on MPCR-TNZ, RGO-MPCR-TNZ, and Dex/RGO-MPCR-TNZ was analyzed by Alizarin red staining using an Osteogenesis Assay Kit (ECM815, Millipore, Bedford, MA) according to the manufacturer's protocol. The relative amount of Alizarin red from MPCR-TNZ, RGO-MPCR-TNZ, and Dex/RGO-MPCR-TNZ was quantified with a microplate reader at OD_{405}. For the analysis of ALP activity, cell lysates were isolated using a cell lysis buffer at day 7 and ALP substrate buffer containing 5 mM of p-nitrophenol (pNP) was added in each group. After incubation at 37 °C for 1 h, the absorbance at 405 nm was measured with a microplate reader. The ALP activity value was normalized by protein content measured at 590 nm after Coomassie blue staining. Osteocalcin immunofluorescence staining was carried out after fixation of each group in 4% formaldehyde solution. Rabbit primary antiosteocalcin antibody and FITC-labeled antirabbit goat secondary antibody were used for the staining. Fluorescence images were obtained with a Leica TCS-SP5-MP-SMD confocal system (Leica Microsystems Wetzlar, Wetzlar, Germany). Real-time quantitative reverse transcription polymerase chain reaction (RT-qPCR) was performed for the analysis of osteogenic gene expression such as runt-related transcription factor 2 (Runx2), osteopontin (OPN), collagen type 1 (Col-1), and osteocalcin (OCN). The amplification primer sequences were as follows: Runx2 (Forward: AAG TGC GGT GCA AAC TTT CT and Reverse: TCT CGG TGG CTG GTA GTG A), OPN (Forward: CTT TCA CTC CAA TCG TCC CTA C and Reverse: CCT TAG ACT CAC CGC TCT TCA T), Col-1 (Forward:

DOI: 10.1021/acsami.5b03431
ACS Appl. Mater. Interfaces 2015, 7, 9598−9607

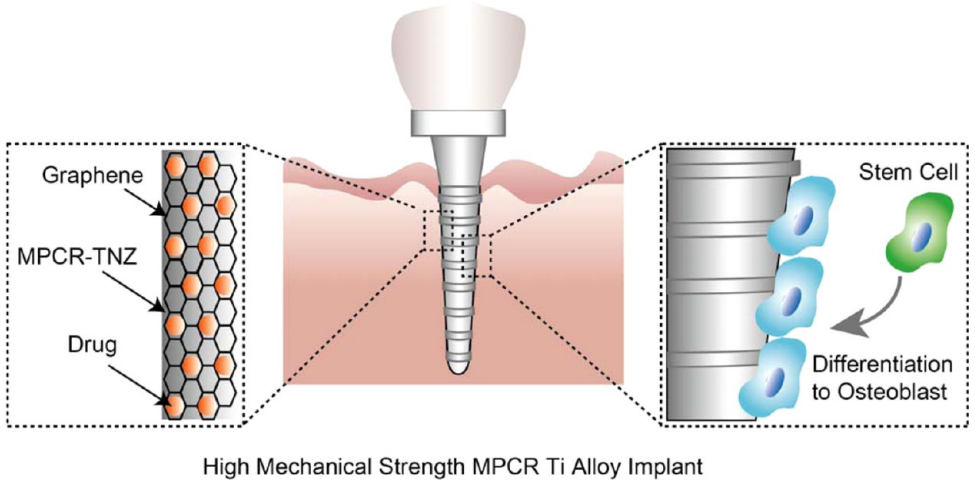

Figure 1. Schematic illustration for multipass caliber-rolled (MPCR) Ti alloy surface-modified with dexamethasone-loaded graphene for minimally invasive application of dental implant with a high mechanical strength and a small diameter.

AGA GCA TGA CCG ATG GAT TC and Reverse: CCT TCT TGA GGT TGC CAG TC), OCN (Forward: GGA CCA TCT TTC TGC TCA CTC TG and Reverse: TTC ACT ACC TTA TTG CCC TCC TG), and GAPDH (Forward: TCG GTG TGA ACG GAT TTG G and Reverse: TCT CCA CTT TGC CAC TGC A). RT-qPCR using Power SYBR Green PCR Master Mix was performed using a CFX-96 real-time PCR detection system (Bio-Rad Laboratories, Hercules, CA).

RGO coating on MPCR-TNZ dental implants. A prototype of MPCR-TNZ dental implant was prepared by machining along the rolling direction, on which RGO was coated as described above. Briefly, the MPCR-TNZ dental implant was immersed in piranha solution for 1 h and then treated with 3% of APTES solution for 1 h. After that, APTES-treated MPCR-TNZ was immersed in 4 mg/mL of GO solution for 30 min on an orbital shaker (Jeiotech, Daejeon, Korea). After removal of unabsorbed GO with a nitrogen gun, the coated GO was reduced in hydrazine vapor.

Dental implantation of RGO-MPCR-TNZ in artificial bone block. A prototype of MPCR-TNZ dental implant was implanted into an artificial bone block provided from Dio Implant Co. (Busan, Korea). Before implantation, tapped hole was formed using an electrical motor drill. The stability of RGO coating on a screw shaped MPCR-TNZ dental implant was analyzed by Raman spectroscopy and SEM before and after implantation.

Dynamic fatigue test of MPCR-TNZ dental implant. Dynamic fatigue test was performed according to ISO 14801. The direction of implant assembly was set to be at an angle of 30 ± 2° from the loading direction. The load varied sinusoidally between a maximum value and 10% of it at a frequency of 2 Hz. All the prototype implant samples were carefully rinsed with ethanol prior to commencing the fatigue test. The test was carried out in PBS media until the fracture occurred. A few samples withstanding 2×10^6 cycles were regarded to be unbreakable under those conditions, as suggested in ISO 14801.

3. RESULTS AND DISCUSSION

3.1. Multipass caliber-rolling of Ti alloys. Figure 1 shows a schematic illustration of a Dex/RGO-MPCR-TNZ implant with a high mechanical strength and a small diameter for minimally invasive dental implantation. The high mechanical strength MPCR-TNZ was surface-modified with RGO and loaded with osteogenic Dex via π - π stacking for effective osseointegration. MPCR Ti alloys were successfully prepared as we reported elsewhere.[7] Then, the microstructure of prepared Ti alloys was investigated by EBSD (Figure 2a). It is well-known that the rapid cooling from a temperature above T_β leads to the full α' martensite.[17,18] In accordance, ST-TNZ was composed of full α' structure. Meanwhile, the reheating of ST-TNZ below T_β decomposed the martensite into α and β phases. Our previous work also revealed the reduction of martensitic transformation in this condition due to the concentration of β-stabilizing elements in the β phase.[7] Hence, STA-TNZ and MPCR-TNZ were consisted with (α + β) two-phase structure. From the viewpoint of grain morphology, similar structure was observed in ST-TNZ and STA-TNZ. Both materials showed a lath structure containing coarse grains (d = 2.1 ± 0.5 μm for ST and d = 1.9 ± 0.4 μm for STA) with the static grain growth and β precipitation. In contrast, MPCR-TNZ was consisted with equiaxed and ultrafine grains (d = 0.3 ± 0.1 μm, average of α and β) due to the dynamic globularization and grain refinement, proving that the UFG structure was successfully induced by the MPCR process.

3.2. Mechanical properties of MPCR Ti alloys. As shown in Figure 2b, tensile properties of various Ti alloys showed obvious differences among the materials. ST-TNZ recorded the lowest yield stress (YS) and ultimate tensile stress (UTS). The aging process subjected to STA-TNZ improved both properties. Moreover, the MPCR process enhanced the mechanical properties even further. The YS and UTS increased by 80% and 45% in MPCR-TNZ, compared to ST-TNZ, respectively. In addition, the hardness of MPCR-TNZ (282.4 ± 4.2 HV) was 25% higher than that of ST-TNZ (225.3 ± 4.8 HV) and similar to that of STA-TNZ (279.6 ± 4.0 HV). The results reflected increasing Young's modulus, as well as strength and hardness, in STA-TNZ and MPCR-TNZ (Figure 2c). Remarkably, the values of Young's modulus were still lower than that of CP-Ti (102−104 GPa) which is a conventionally used metallic biomaterial.[19] It should also be noted that MPCR-TNZ had a similar Young's modulus in comparison to STA-TNZ despite its higher strength.

The ratio of YS to Young's modulus, called mechanical compatibility, has been utilized to evaluate the comprehensive mechanical properties required for biomedical applications.[20−22] The mechanical compatibilities were analyzed for the tested alloys as well as the conventional metallic biomaterials (Figure 2d).[19,23] Ti alloys, including ST-TNZ, generally provided good mechanical compatibilities around 8×10^{-3}, whereas Co−Cr−Mo alloy, 316L stainless steel, and CP-Ti recorded lower values. STA-TNZ showed higher mechanical compatibility than these materials. Moreover, MPCR-TNZ

DOI: 10.1021/acsami.5b03431
ACS Appl. Mater. Interfaces 2015, 7, 9598−9607

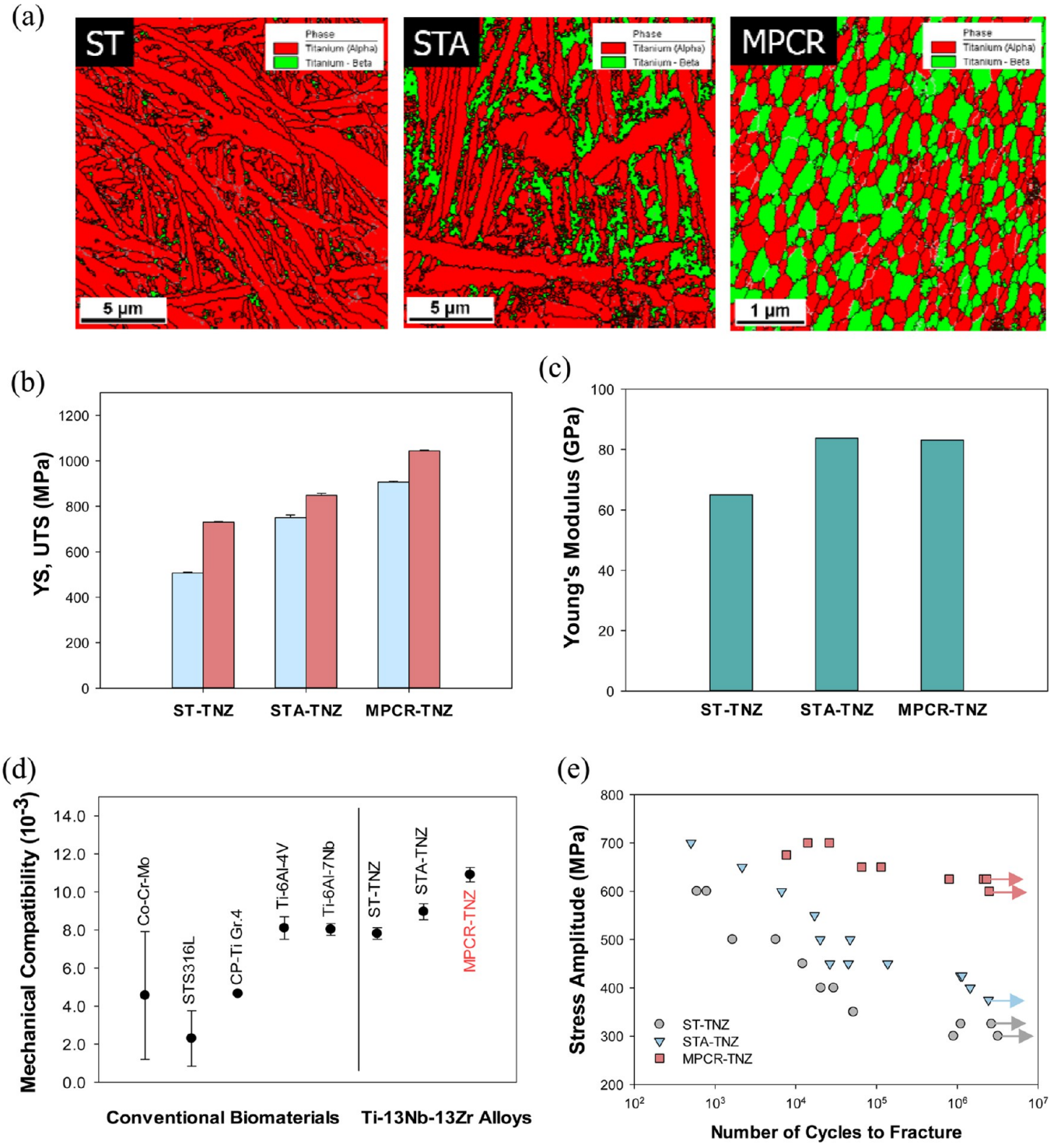

Figure 2. Microstructures and mechanical properties of Ti alloys. (a) EBSD phase map of ST-TNZ, STA-TNZ, and MPCR-TNZ where red and green areas indicate α/α' and β, respectively. (b) Uniaxial tensile properties where blue and red bars indicate YS and UTS, respectively. (c) Young's moduli measured by free resonance method. (d) Mechanical compatibilities of the present and conventional biomaterials. (e) A diagram of stress amplitude vs number of cycles to fracture showing the fatigue resistance. Arrows indicate no fracture until a number of cycles of 2×10^6.

exhibited the best mechanical compatibility of 11×10^{-3} due to the significantly enhanced strength and maintained Young's modulus similar to that of STA-TNZ. The superior mechanical properties of MPCR-TNZ can be interpreted in light of the microstructural characteristics. First, the UFG structure generated a number of barriers to dislocation movement, resulting in the considerable grain-boundary strengthening.[24] Second, the $(\alpha + \beta)$ phase structure provided the higher strength and hardness than α' martensite comprising ST-TNZ.[7] In contrast to strength, Young's modulus of material is not influenced by a grain size,[25] which explains the comparable Young's moduli between STA-TNZ and MPCR-TNZ despite their different strengths. The result implies the advantage of

DOI: 10.1021/acsami.5b03431
ACS Appl. Mater. Interfaces 2015, 7, 9598−9607

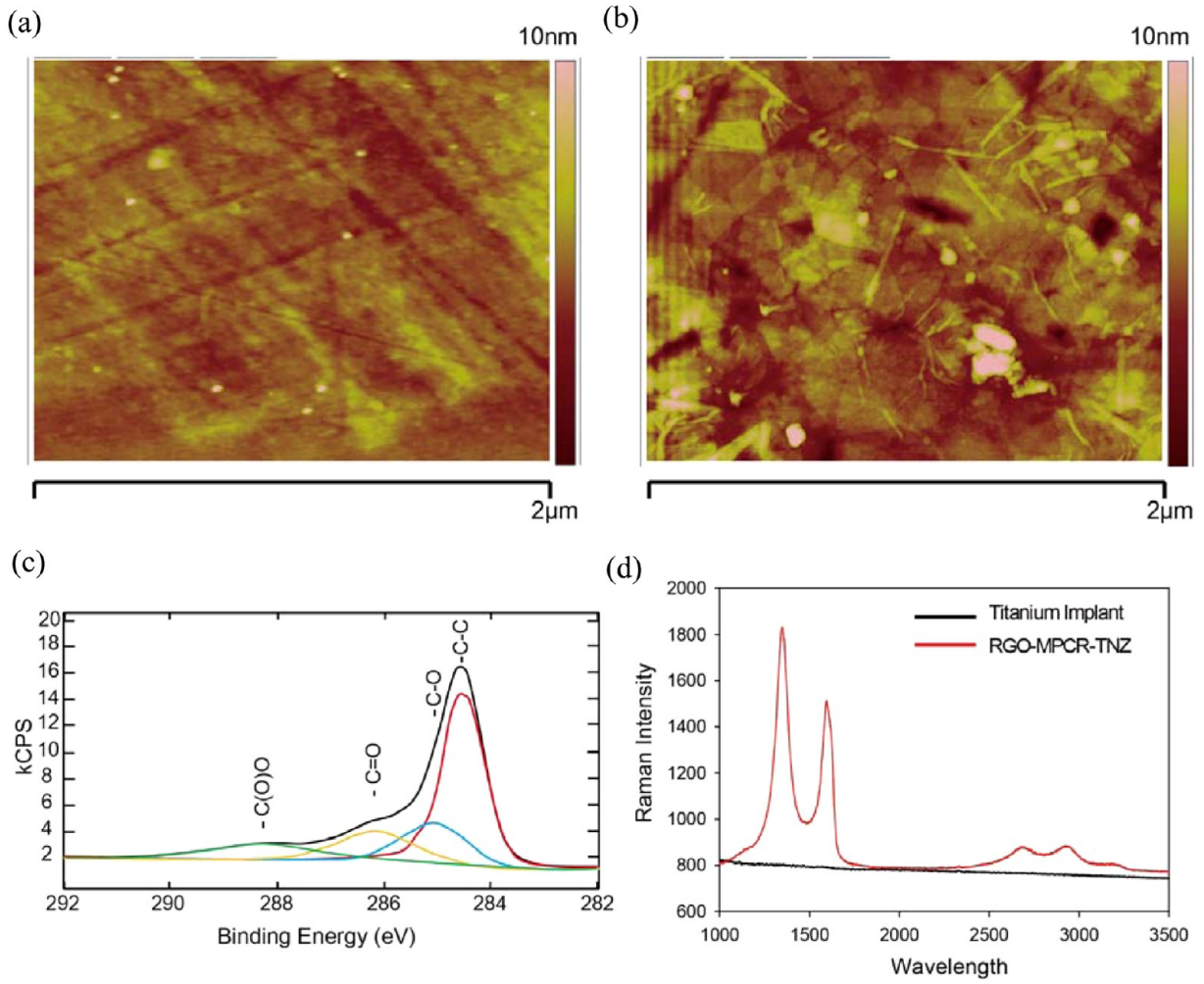

Figure 3. Atomic force microscopy of (a) polished MPCR-TNZ and (b) RGO-MPCR-TNZ. (c) X-ray photoelectron spectroscopy of RGO-MPCR-TNZ at carbons. (d) Raman spectroscopy of MPCR-TNZ and RGO-MPCR-TNZ.

MPCR process which strengthens a material without increasing Young's modulus further.

Fatigue resistance of the investigated materials was analyzed using the diagram of stress amplitude vs number of cycles to fracture (Figure 2e). Similar with other mechanical properties, MPCR-TNZ exhibited a notably high-cycle fatigue resistance in the entire range of interests. The fatigue limit, at which a sample was not fractured until a loading cycle of 2×10^6, was determined to be 600 MPa. This performance was superior to those of ST-TNZ (300 MPa) and STA-TNZ (375 MPa). The high-cycle fatigue life correlates with the material strength in general.[26,27] An increased strength enhances a resistance against fatigue fracture by retarding a crack initiation at surface or subsurface regions.[27] This is in good agreement with the positive correlation between the fatigue limit and strength for the investigated TNZ alloys. Thus, the superior resistance to high-cycle fatigue fracture in MPCR-TNZ might result from its enhanced mechanical strength.

3.3. Preparation and characterization of RGO-MPCR-TNZ. After APTES functionalization on piranha-treated MPCR-TNZ, negatively charged GO was electrostatically adhered on positively charged MPCR-TNZ surface. Then, GO-coated MPCR-TNZ was chemically reduced in hydrazine vapor to obtain RGO-MPCR-TNZ. AFM image in Figure 3b shows the same sheet morphology with the graphene structure on MPCR-TNZ surface, which was not observed in the polished surface (Figure 3a). XPS analysis at carbon atoms on RGO-MPCR-TNZ showed the successful coating of RGO including C−C, C−O, C═O, and O−C═O peaks (Figure 3c). Raman spectroscopy of RGO-MPCR-TNZ showed the D band at 1350 cm^{-1} and G band at 1580 cm^{-1}, whereas no significant Raman signal was observed in the case of MPCR-TNZ (Figure 3d).

Contact angle was measured on ST-TNZ, STA-TNZ, MPCR-TNZ, and RGO-MPCR-TNZ (Figure S1). No significant difference in contact angle was observed among the bare materials. However, RGO-MPCR-TNZ exhibited a considerable increase in the contact angle due to the hydrophobic surface characteristics of RGO on MPCR-TNZ. After incubation of RGO-MPCR-TNZ in serum for 2 h, hydrophobic RGO surface became hydrophilic, providing a preferable condition for cells. All these data confirmed the successful RGO coating on MPCR-TNZ.

3.4. MC3T3-E1 cell viability, attachment, and growth. The cytocompatibility of ST-TNZ, STA-TNZ, and MPCR-TNZ with and without RGO coating was assessed by MTT assay after culture of MC3T3-E1 cells on each sample for 3 days. The RGO coated MPCR-TNZ showed slightly higher cell viability without cytotoxicity than that of MPCR-TNZ (Figure 4a). The RGO coating on Ti alloys enhanced cell viability

DOI: 10.1021/acsami.5b03431
ACS Appl. Mater. Interfaces 2015, 7, 9598−9607

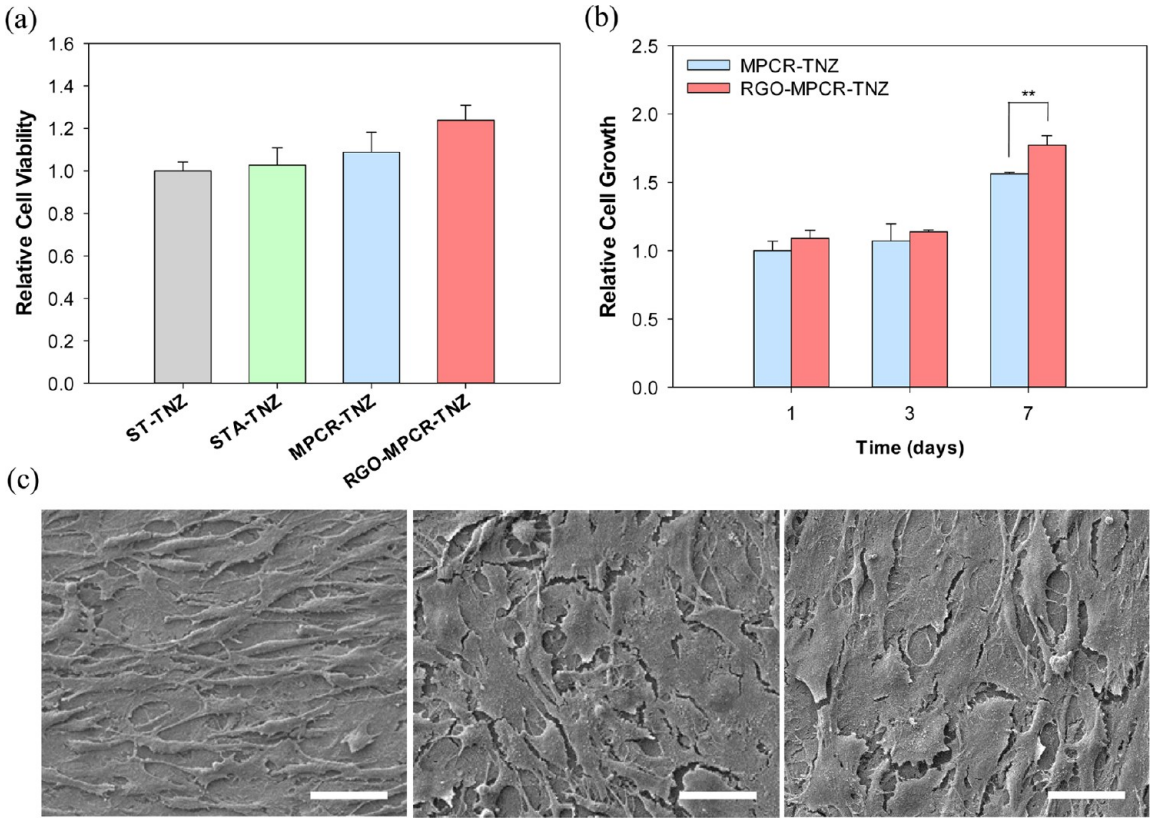

Figure 4. (a) Relative cell viability on ST-TNZ, STA-TNZ, MPCR-TNZ, and RGO-MPCR-TNZ after culture for 3 days. (b) MC3T3-E1 cell proliferation on MPCR-TNZ and RGO-MPCR-TNZ after culture for 1 day, 3 days, and 7 days. (c) SEM of MC3T3-E1 cells cultured on MPCT-TNZ, RGO-MPCR-TNZ, and Dex/RGO-MPCR-TNZ from left to right for 7 days (scale bar = 50 μm).

despite its hydrophobic surface characteristics with a contact angle of 77.6°. It is well-known that hydrophilic surface is biocompatible compared to hydrophobic surface. However, in the case of RGO coating, the rapid adsorption of serum protein on graphene surface induces hydrophilic, cell-adhesive, and biocompatible microenvironment.[28] Indeed, the contact angle after the adsorption of serum protein was considerably decreased to 41.3° (Figure S1).

Chemicals or protein drugs can be easily loaded on graphene surface by $\pi-\pi$ stacking for effective osseointegration. For example, Dex can be loaded as a gene regulating chemical drug to induce osteogenic differentiation by increasing the transcription of four and a half LIM domains 2 (FHL-2). The loading efficiency of Dex on RGO-MPCR-TNZ was 31% after drug loading for 24 h. Dex dissolved in DMSO showed a main absorbance peak at 260 nm (Figure S2a). *In vitro* drug release from RGO-MPCR-TNZ immersed in PBS at 37 °C was monitored for a week. Because Dex is a hydrophobic drug, only 10% of total loaded Dex was released for a week, remaining on RGO-MPCR-TNZ (Figure S2b). The stably loaded Dex on RGO-MPCR-TNZ might induce long-term stimulation of stem cells on RGO-MPCR-TNZ for osseointegration postimplantation. The high local concentration of Dex on the surface is reported to facilitate osteogenesis.[13]

The proliferation of undifferentiated MC3T3-E1 cells cultured on MPCR-TNZ and RGO-MPCR-TNZ for 1 day, 3 days, and 7 days was also monitored by MTT assay (Figure 4b). The MC3T3-E1 cells could grow and proliferate more significantly on RGO-MPCR-TNZ than MPCR-TNZ. The results indicate that coating alone with RGO did significantly improve cell proliferation, additionally making possible the controlled drug release. The cell morphology and attachment of MC3T3-E1 cells on MPCR-TNZ, RGO-MPCR-TNZ, and Dex/RGO-MPCR-TNZ were visualized by SEM after culture for 7 days. The cells cultured on DEX/RGO-MPCR-TNZ and RGO-MPCR-TNZ showed well spread and flat morphologies, whereas cells cultured on MPCR-TNZ showed rod like and relatively elongated shapes (Figure 4c).

3.5. Differentiation of MC3T3-E1 progenitor cells. It is important to facilitate the differentiation of stem cells into osteoblasts on the surface of implant for osseointegration after implantation surgery. Drug preloaded implant can be used as an effective strategy for osseointegration. In particular, graphene can be loaded with a hydrophobic osteogenic inducer of Dex to increase the local concentration on the surface, resulting in relatively fast and effective cell differentiation. The facilitated differentiation of progenitor cells into osteoblasts was confirmed by Alizarin red staining, immunofluorescence imaging, alkaline phosphatase activity test, and RT-qPCR. MC3T3-E1 cells cultured for 7 days on Dex/RGO-MPCR-TNZ and RGO-MPCR-TNZ exhibited a significant improvement in calcium-nodule formation compared to MPCR-TNZ (Figure 5a). Confocal scanning laser microscopy showed remarkable osteocalcin expression in cells on Dex/RGO-MPCR-TNZ, whereas cells on RGO-MPCR-TNZ and MPCR-TNZ were partially differentiated and nondifferentiated (Figure 5b). On the other hand, cells cultured on MPCR-TNZ, RGO-MPCR-TNZ, and Dex/RGO-MPCR-TNZ in nonosteogenic media exhibited relatively insufficient osteogenic tendency (Figure S3). For the quantitative analysis of Alizarin

DOI: 10.1021/acsami.5b03431
ACS Appl. Mater. Interfaces 2015, 7, 9598−9607

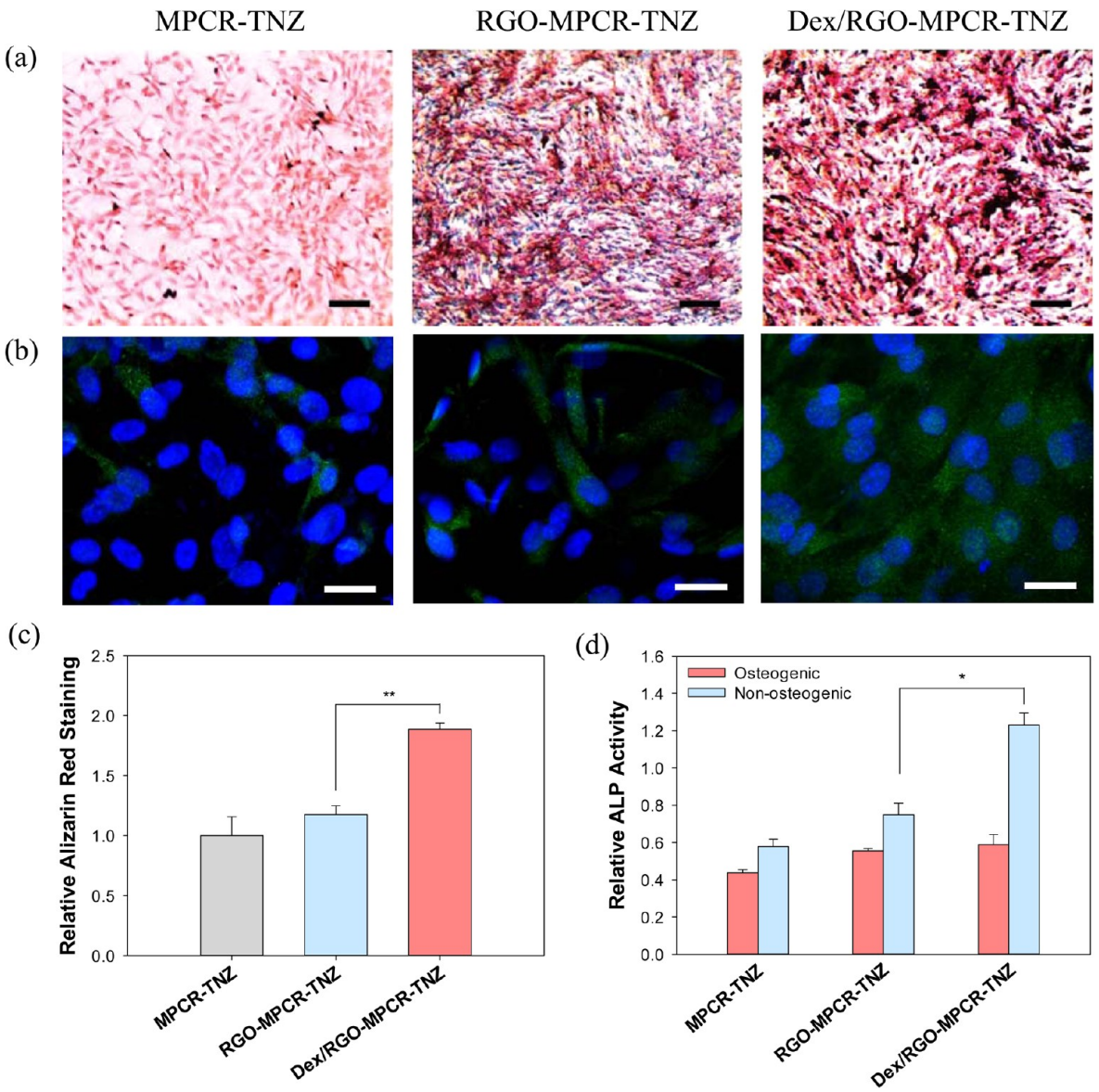

Figure 5. (a) Alizarin red staining and (b) immunofluorescence of osteocalcin in MC3T3-E1 cells cultured on MPCR-TNZ, RGO-MPCR-TNZ, and Dex/RGO-MPCR-TNZ in osteogenic media (scale bar: black = 500 μm, white = 25 μm). (c) Relative quantification of Alizarin red staining normalized with the MPCR-TNZ group. (d) ALP activities of cells cultured on each sample in osteogenic and nonosteogenic medium.

red staining, the stained cells were harvested and analyzed with a microplate reader at OD_{405} according to the manufacturer's protocol. As shown in Figure 5c, Dex/RGO-MPCR-TNZ group showed the most significant calcium nodule deposition. In addition, cells cultured in osteogenic media showed enhanced ALP activity compared to cells cultured in non-osteogenic media (Figure 5d). The cells on Dex/RGO-MPCR-TNZ showed the highest ALP activity among all the other groups.

The differentiation of MC3T3-E1 cells in each group was quantitatively analyzed by RT-qPCR using osteogenic expression markers such as Runx2, OPN, Col-1, OCN, and GAPDH as a housekeeping gene (Figure 6). The relative mRNA expression was calculated using competitive Ct methods and the expression levels were normalized with respect to the control cells differentiated on tissue culture polystyrene dish (TCPS). MC3T3-E1 cells cultured on Dex/RGO-MPCR-TNZ showed obviously higher expression levels of Runx2, OPN, Col-1, and OCN than those grown on RGO-MPCR-TNZ, MPCR-TNZ and TCPS. The expression levels of Runx2, OPN, and OCN from the cells cultured on MPCR-TNZ were comparable to those of TCPS, whereas Col-1 showed a lower expression level than that of TCPS. All these results confirmed and supported the successful and facilitated progenitor cell differentiation of MC3T3-E1 cells into osteoblasts on Dex/RGO-MPCR-TNZ.

3.6. Implantation of RGO-MPCR-TNZ into artificial bone block. For further applications, a prototype of dental implant was prepared using MPCR-TNZ, which was surface-modified with RGO. RGO could be easily coated on the surface of MPCR-TNZ regardless of the material shape using the solution dipping method. The prototype implant of RGO-MPCR-TNZ was successfully implanted onto an artificial bone block having similar mechanical and structural properties with jawbone (Figure 7a). The RGO surface-modified on MPCR-TNZ was characterized by Raman spectroscopy before and after implantation. Typical D band and G band peaks were observed from RGO-MPCR-TNZ, whereas MPCR-TNZ

DOI: 10.1021/acsami.5b03431
ACS Appl. Mater. Interfaces 2015, 7, 9598−9607

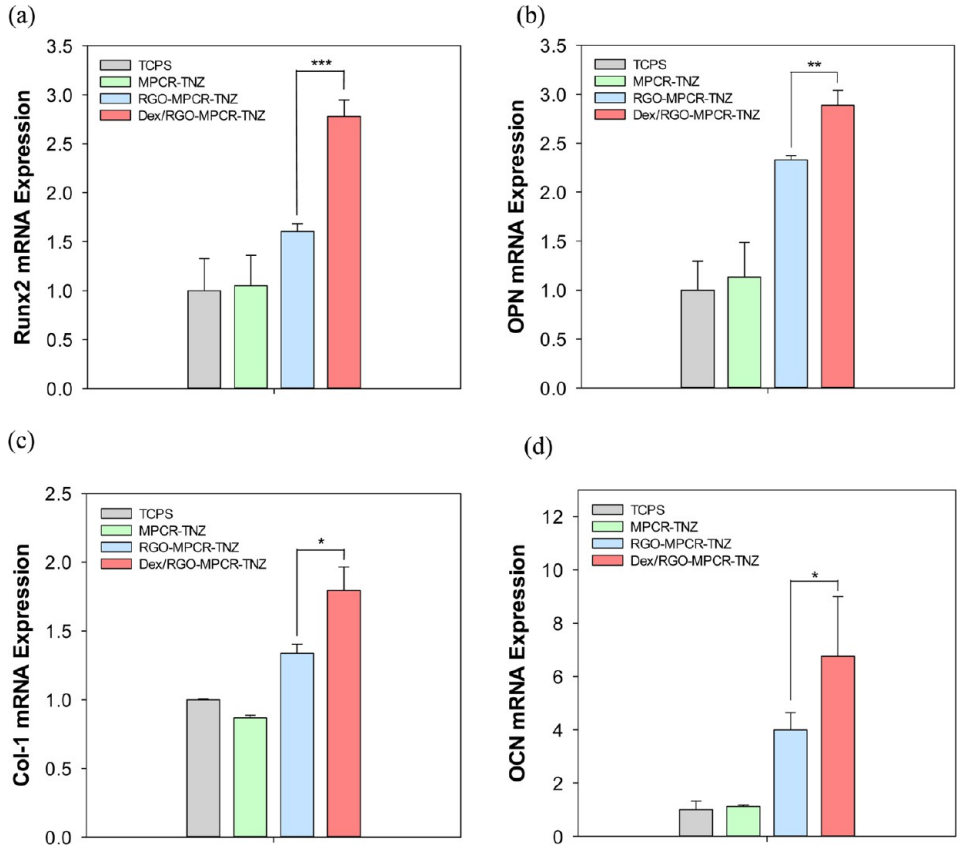

Figure 6. RT-qPCR analysis of (a) Runx2, (b) OPN, (c) Col-1, and (d) OCN of MC3T3-E1 cells differentiated on MPCR-TNZ, RGO-MPCR-TNZ, and Dex/RGO-MPCR-TNZ. The data shown are mean mRNA expression levels relative to GAPDH expression. The expression levels are normalized with respect to the expression level of cells grown on TCPS.

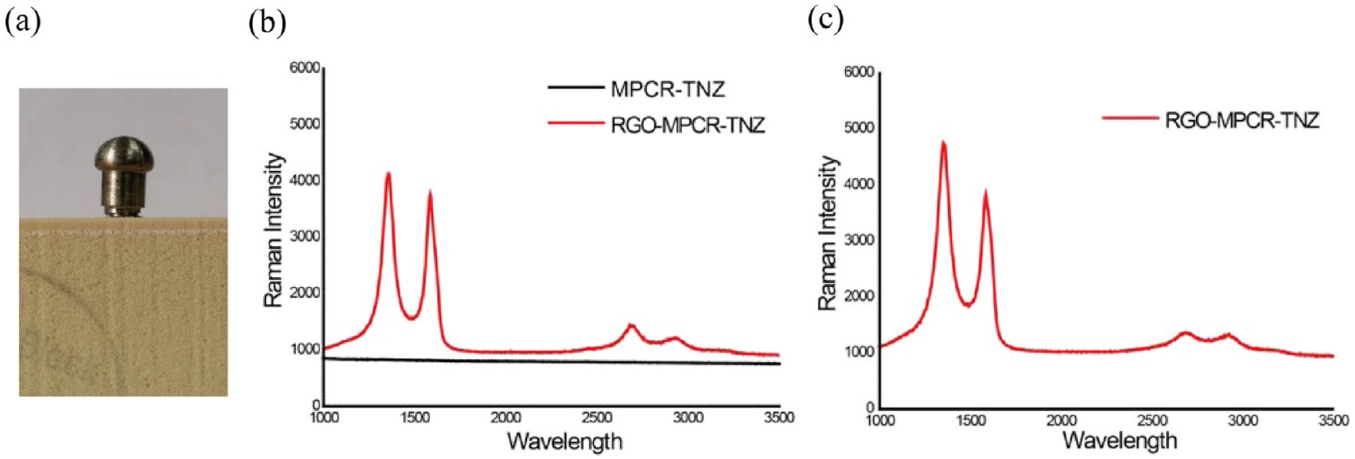

Figure 7. (a) Photoimage showing the implantation of a prototype implant prepared with RGO-MPCR-TNZ to an artificial bone block. Raman spectroscopy of a prototype implant prepared with (b) MPCR-TNZ or RGO-MPCR-TNZ, and (c) RGO-MPCR-TNZ recovered after implantation.

showed no observable peaks (Figure 7b). More importantly, the typical RGO Raman peak was also observed from RGO-MPCR-TNZ recovered after implantation (Figure 7c). In addition, the RGO coating on MPCR-TNZ was analyzed by SEM. As shown in Figure 8, the remaining RGO in a sheet-structure was observed on the surface of RGO-MPCR-TNZ. In contrast, MPCR-TNZ showed only machining scratches on the surface (Figure 8). The stable RGO on the prototype implant of MPCR-TNZ even after implantation confirmed the feasibility of RGO-MPCR-TNZ for clinical dental applications.

The dynamic fatigue property of implant materials is one of the important factors because a dental implant is directly exposed to consistent masticatory movement. Although the fatigue resistance of MPCR-TNZ was confirmed to be superior in the uniaxial mode (Figure 2e), an implant is also required to endure multiaxial loads in most clinical cases. It is noted that fatigue property can vary depending on the experimental environment (*e.g.*, in the air or in the aqueous solution). Accordingly, dynamic fatigue property of RGO-MPCR-TNZ was evaluated under the physiological condition (in PBS at 37

DOI: 10.1021/acsami.5b03431
ACS Appl. Mater. Interfaces 2015, 7, 9598−9607

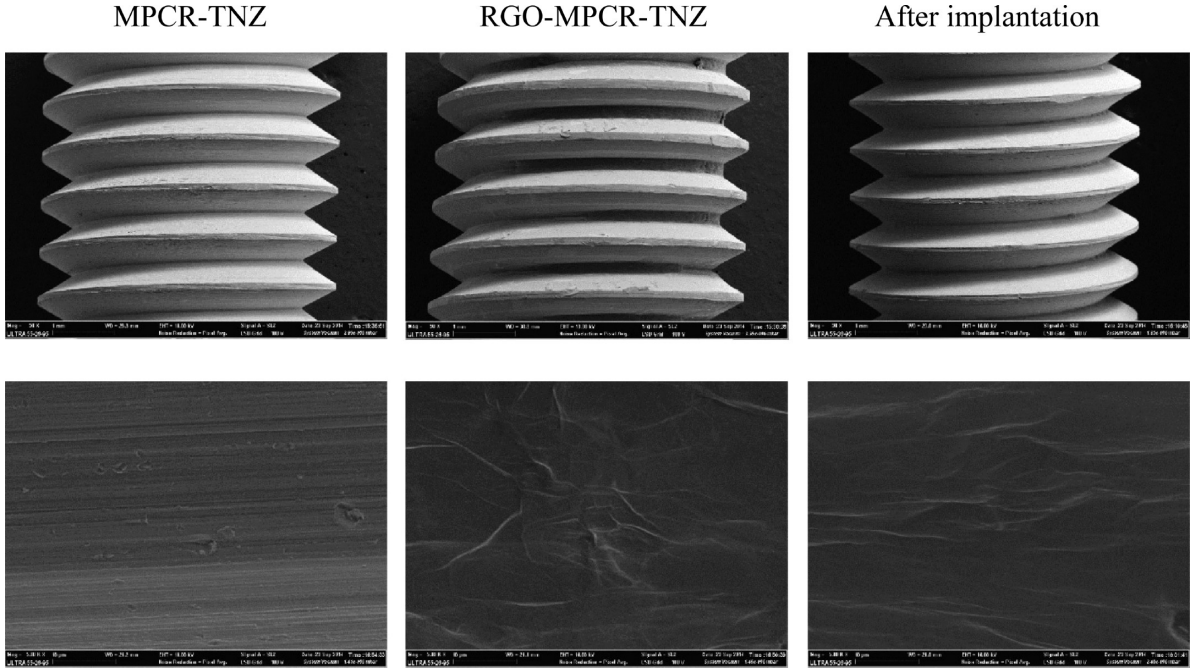

Figure 8. Scanning electron microscopy of a prototype implant prepared with MPCR-TNZ and RGO-MPCR-TNZ, and RGO-MPCR-TNZ recovered after implantation (top: × 50, bottom: × 5000).

°C) to confirm the enhanced mechanical properties in the form of actual dental implant. As shown in Figure 9, the implant

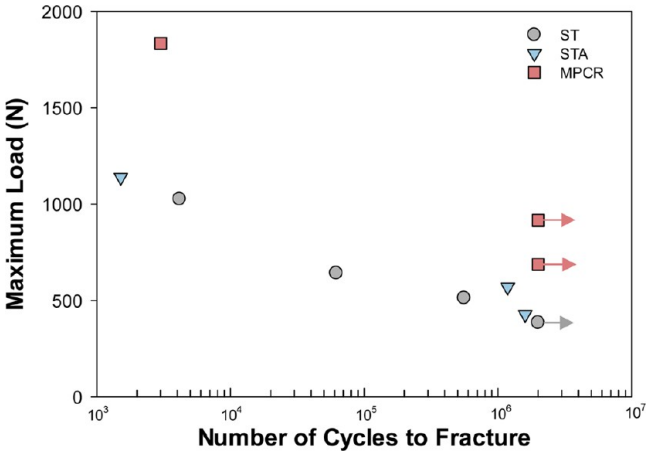

Figure 9. Dynamic fatigue properties of a prototype implant in a biological condition. The arrows indicate that sample was not fractured until a number of cycles of 2×10^6.

prototype of RGO-MPCR-TNZ exhibited superior fatigue resistance to ST and STA groups. RGO-MPCR-TNZ resisted a fatigue load of 916 N or less until a number of cycles of 2×10^6, whereas ST-TNZ and STA-TNZ easily fractured under the same conditions. These results indicate that the implant material developed in this work has a remarkable resistance to fatigue fracture in both uniaxial and multiaxial conditions.

In a viewpoint of dental implantation, the improvement of mechanical properties is an important issue because a small-sized implant is required for patients who have insufficient bone or gum tissues for implantation. The Dex/RGO-MPCR-TNZ implant fixture with a diameter of 2 mm can sustain the same amount of load taken by the conventional 3 mm Ti product due to the two times higher strength. The dynamic fatigue experiment in physiological condition proved the superior fatigue resistance of the implant prototype, reflecting the enhanced mechanical stability and the possibility of prolonged product lifetime. RGO coating on Ti surface could be easily performed not only on 2D flat surface but also on 3D structure, especially screw shaped implant. The drug-loaded implant materials can stimulate and facilitate cellular response around implant surface to reduce the osseointegration time. The RGO coating strategy on Ti alloys with controlled drug delivery is expected to be applied for various dental and biomedical applications.

4. CONCLUSION

We successfully prepared a high mechanical strength Ti alloy using the MPCR process for dental applications. The strength of MPCR-TNZ increased considerably, maintaining the Young's modulus in a similar level with that of the conventional STA-TNZ. The surface of MPCR-TNZ was easily modified with RGO and loaded with an ostegoenic chemical drug of Dex by $\pi-\pi$ stacking. The drug loaded RGO-MPCR-TNZ resulted in effective and facilitated differentiation of MC3T3-E1 cells to osteoblasts, showing remarkable expression of ostegenic expression markers such as Runx2, OPN, Col-1, and OCN. Also, RGO-MPCR-TNZ showed enhanced calcium nodule deposition and ALP activity. The implantation of a prototype dental implant prepared with RGO-MPCR-TNZ to an artificial bone block revealed the feasibility of stable RGO surface modification for further applications. The high mechanical strength dental implant of Dex/RGO-MPCR-TNZ can be effectively applied to minimally invasive dental implantation.

■ ASSOCIATED CONTENT

Supporting Information

Additional information on materials, *in vitro* drug release test of dexamethasone, Alizarin red staining, and immunocytochemistry of osteocalcin in nonosteogenic media. The Supporting

DOI: 10.1021/acsami.5b03431
ACS Appl. Mater. Interfaces 2015, 7, 9598−9607

Information is available free of charge on the ACS Publications website at DOI: 10.1021/acsami.5b03431.

AUTHOR INFORMATION

Corresponding Authors

*Tel.: +82 54 279 2159; Fax: +82 54 279 2399; E-mail: skhanb@postech.ac.kr (S. K. Hahn).

*Tel.: +82 54 279 9001; Fax: +82 54 279 9099; E-mail: cslee@postech.ac.kr (C. S. Lee).

Author Contributions

§H.S.J. and T.L. contributed equally to this work.

Notes

The authors declare no competing financial interest.

ACKNOWLEDGMENTS

Artificial bone block was kindly gifted from DIO Implant Co. We thank H. Kim and K. Cho for Raman spectroscopic analysis. This work was financially supported by POSCO. This work was financially supported by the Midcareer Researcher Program and Bio & Medical Technology Development Programs (Project No. 2012R1A2 A2A06045773 and 2012M3A9C6049791) of the National Research Foundation funded by the Korean government (MEST).

REFERENCES

(1) Schiff, N.; Grossgogeat, B.; Lissac, M.; Dalard, F. Influence of Fluoride Content and pH on the Corrosion Resistance of Titanium and its Alloy. *Biomaterials* **2002**, *23*, 1995−2002.

(2) Kimura, Y.; Inoue, T.; Yin, F.; Tsuzaki, K. Inverse Temperature Dependence of Toughness in an Ultrafine Grain-Structure Steel. *Science* **2008**, *320*, 1057−1060.

(3) Lee, T.; Park, C. H.; Lee, D. L.; Lee, C. S. Enhancing Tensile Properties of Ultrafine-grained Medium-carbon Steel Utilizing Fine Carbides. *Mater. Sci. Eng., A* **2011**, *528*, 6558−6564.

(4) Lee, T.; Park, C. H.; Lee, S. Y.; Son, I. H.; Lee, D. L.; Lee, C. S. Mechanisms of Tensile Improvement in Caliber-rolled High-carbon Steel. *Met. Mater. Int.* **2012**, *18*, 391−396.

(5) Lee, T.; Koyama, M.; Tsuzaki, K.; Lee, Y. H.; Lee, C. S. Tensile Deformation Behavior of Fe-Mn-C TWIP Steel with Ultrafine Elongated Grain Structure. *Mater. Lett.* **2012**, *75*, 169−171.

(6) Koyama, M.; Lee, T.; Lee, C. S.; Tsuzaki, K. Grain Refinement Effect on Cryogenic Tensile Ductility in a Fe−Mn−C Twinning-induced Plasticity Steel. *Mater. Des.* **2013**, *49*, 234−241.

(7) Lee, T.; Heo, Y. U.; Lee, C. S. Microstructure Tailoring to Enhance Strength and Ductility in Ti−13Nb−13Zr for Biomedical Applications. *Scr. Mater.* **2013**, *69*, 785−788.

(8) Dikin, D. A.; Stankovich, S.; Zimney, E. J.; Piner, R. D.; Dommett, G. H. B.; Evmenenko, G.; Nguyen, S. T.; Ruoff, R. S. Preparation and Characterization of Graphene Oxide Paper. *Nature* **2007**, *448*, 457−460.

(9) Loh, K. P.; Bao, Q.; Eda, G.; Chhowalla, M. Graphene Oxide as a Chemically Tunable Platform for Optical Applications. *Nat. Chem.* **2010**, *2*, 1015−1024.

(10) Jung, H. S.; Lee, M. Y.; Kong, W. H.; Do, I. H.; Hahn, S. K. Nano Graphene Oxide-hyaluronic acid Conjugate for Target Specific Cancer Drug Delivery. *RSC Adv.* **2014**, *4*, 14197−14200.

(11) Yang, W. R.; Ratinac, K. R.; Ringer, S. P.; Thordarson, P.; Gooding, J. J.; Braet, F. Carbon Nanomaterials in Biosensors: Should You Use Nanotubes or Graphene? *Angew. Chem., Int. Ed.* **2010**, *49*, 2114−2138.

(12) Park, S. Y.; Park, J.; Sim, S. H.; Sung, M. G.; Kim, K. S.; Hong, B. H.; Hong, S. H. Enhanced Differentiation of Human Neural Stem Cells into Neurons on Graphene. *Adv. Mater.* **2011**, *23*, H263−H267.

(13) Lee, W. C.; Lim, C. H.; Shi, H.; Tang, L. A.; Wang, Y.; Lim, C. T.; Loh, K. P. Origin of Enhanced Stem Cell Growth and Differentiation on Graphene and Graphene Oxide. *ACS Nano* **2011**, *5*, 7334−7341.

(14) Nayak, T. R.; Andersen, H.; Makam, V. S.; Khaw, C.; Bae, S.; Xu, X.; Ee, P. L. R.; Ahn, J. H.; Hong, B. H.; Pastorin, G.; Özyilmaz, B. Graphene for Controlled and Accelerated Osteogenic Differentiation of Human Mesenchymal Stem Cells. *ACS Nano* **2011**, *5*, 4670−4678.

(15) Wu, C.; Miron, R.; Sculeaan, A.; Kaskel, S.; Doert, T.; Schulze, R.; Zhang, Y. Proliferation, Differentiation and Gene Expression of Osteoblasts in Boron-containing Associated with Dexamethasone Deliver from Mesoporous Bioactive Glass Scaffolds. *Biomaterials* **2011**, *32*, 7068−7078.

(16) Park, C. H.; Park, J. W.; Yeom, J. T.; Chun, Y. S.; Lee, C. S. Enhanced Mechanical Compatibility of Submicrocrystalline Ti-13Nb-13Zr Alloy. *Mater. Sci. Eng., A* **2010**, *527*, 4914−4919.

(17) Geetha, M.; Singh, A. K.; Gogia, A. K.; Asokamani, R. Effect of Thermomechanical Processing on Evolution of Various Phases in Ti−Nb−Zr Alloys. *J. Alloys Compd.* **2004**, *384*, 131−144.

(18) Lin, C. W.; Ju, C. P.; Chern Lin, J. H. A Comparison of the Fatigue Behavior of Cast Ti−7.5Mo with c.p. Titanium, Ti−6Al−4V and Ti−13Nb−13Zr Alloys. *Biomaterial* **2005**, *26*, 2899−2907.

(19) Niinomi, M. Mechanical Properties of Biomedical Titanium Alloys. *Mater. Sci. Eng., A* **1998**, *243*, 231−236.

(20) Song, Y.; Xu, D. S.; Yang, R.; Li, D.; Wu, W. T.; Guo, Z. X. Theoretical Study of the Effects of Alloying Elements on the Strength and Modulus of β-type Bio-titanium Alloys. *Mater. Sci. Eng., A* **1999**, *260*, 269−274.

(21) Zhou, Y. L.; Niinomi, M. Microstructures and Mechanical Properties of Ti-50 mass% Ta Alloy for Biomedical Applications. *J. Alloys Compd.* **2008**, *466*, 535−542.

(22) Zhou, Y. L.; Niinomi, M. Ti-25Ta Alloy with the Best Mechanical Compatibility in Ti-Ta Alloys for Biomedical Applications. *Mater. Sci. Eng., C* **2009**, *29*, 1061−1065.

(23) Long, M.; Rack, H. J. Titanium Alloys in Total Joint Replacement—A Materials Science Perspective. *Biomaterial* **1998**, *19*, 1621−1639.

(24) Dieter, G. E. *Mechanical Metallurgy*, SI Metric Edition; McGraw-Hill: London, 1988.

(25) Hao, Y.; Yang, R.; Niinomi, M.; Kuroda, D.; Zhou, Y.; Fukunaga, K.; Suzuki, A. Young's Modulus and Mechanical Properties of Ti-29Nb-13Ta-4.6Zr in Relation to α'' martensite. *Metall. Mater. Trans. A* **2002**, *33*, 3137−3144.

(26) Vinogradov, A. Y.; Stolyarov, V. V.; Hashimoto, S.; Valiev, R. Z. Cyclic Behavior of Ultrafine-grain Titanium Produced by Severe Plastic Deformation. *Mater. Sci. Eng., A* **2001**, *318*, 163−173.

(27) Kim, W. J.; Hyun, C. Y.; Kim, H. K. Fatigue Strength of Ultrafine-grained Pure Ti after Severe Plastic Deformation. *Scr. Mater.* **2006**, *54*, 1745−1750.

(28) Liu, J. B.; Fu, S. H.; Yuan, B.; Li, Y. L.; Deng, Z. X. Toward a Universal Adhesive Nanosheet" for the Assembly of Multiple Nanoparticles Based on a Protein-Induced Reduction/Decoration of Graphene Oxide. *J. Am. Chem. Soc.* **2010**, *132*, 7279−7281.

DOI: 10.1021/acsami.5b03431
ACS Appl. Mater. Interfaces 2015, 7, 9598−9607